BNL-213578-2020-JAAM

Carbon Monoxide Adsorption on Manganese Oxide / Cobalt: An Ambient Pressure X-ray Photoelectron Spectroscopy Study

B. Eren, A. R. Head

To be published in "The Journal of Physical Chemistry C"

January 2020

Center for Functional Nanomaterials

Brookhaven National Laboratory

U.S. Department of Energy

USDOE Office of Science (SC), Basic Energy Sciences (BES) (SC-22)

DISCLAIMER

Carbon Monoxide Adsorption on Manganese Oxide / Cobalt: An Ambient Pressure X-ray Photoelectron Spectroscopy Study

Baran Eren,*,†, Ashley R. Head,**,‡

†*Department of Chemical and Biological Physics, Weizmann Institute of Science, 234 Herzl Street, 76100 Rehovot, Israel,*

‡*Center for Functional Nanomaterials, Brookhaven National Laboratory, Upton, NY 11973, United States of America*

* E-mail: baran.eren@weizmann.ac.il Phone: +972 8-934-3708

** E-mail: ahead@bnl.gov Phone: +1 631 344-3245

Abstract

MnO_x enhances the catalytic activity of Co during Fischer-Tropsch synthesis, increases selectivity towards C_{5+} products, and decreases methane formation. These desired traits are thought to result from a higher CO adsorption energy and, thus, potentially higher CO coverage. To investigate this, ambient pressure X-ray photoelectron spectroscopy (APXPS) was used to probe the CO coverage of a Co foil with increasing MnO_x amounts at room temperature. The technique permits the quantification of chemical species on a surface from ultra-high vacuum to the mbar pressure regime. CO was found to adsorb at both Co and MnO_x sites. The electronic effect which results in the promotion of CO adsorption, also promotes the adsorption of OH groups from background water vapor pressures. This process competes with CO adsorption, despite the water pressure being ~8 orders of magnitude lower than the CO pressure at 1 mbar. Since water is a product of Fisher-Tropsch synthesis, this result has relevance to the understanding of MnO_x as a promoter. This finding highlights the importance of considering unexpected contributions of background impurities in APXPS and other ambient pressure surface science techniques.

1. Introduction

Fischer–Tropsch synthesis (FTS) is an alternative way to produce petroleum-products for transportation fuel from non-petroleum feedstocks. The process converts a mixture of carbon monoxide and hydrogen, also known as synthesis gas, into hydrocarbons using a catalyst.[1-3] The possible hydrocarbon product distribution includes methane (C_1), petroleum gas (C_2-C_4), gasoline (C_5-C_{11}), diesel (C_{12}-C_{20}), and wax (C_{21+}), where gasoline and diesel are the desired products. Petroleum gas and wax can be converted to these sought-after products via oligomerization or cracking, respectively, but methane production is simply a loss of carbon which could otherwise be converted into liquid hydrocarbons and is highly undesirable. Co is one of the best catalysts used in commercial FTS due to its superior activity, high selectivity towards diesel and wax, and low water-gas shift activity, despite its more expensive price compared to highly catalytic Fe.[4-5] In the catalysis science community, many recent works have focused on optimizing the conditions for maximizing C_{5+} formation using Co catalysts. The general operating conditions need the 200-240 °C temperature range, pressures above 10 bar, and hydrogen-rich conditions (typically at 2:1 H_2 to CO ratio) in order to increase the selectivity towards C_{5+} products and disfavor methane formation.[6-7]

Previously, we used ambient pressure x-ray photoelectron spectroscopy (APXPS) in the mbar pressure range to understand the CO and H_2 adsorption and co-adsorption trends on a polycrystalline Co foil, as well as effects of water (a by-product of FTS) and typical impurities.[8] Despite still being four orders of magnitude lower than the desired pressure range used in industrial processes, such studies can help to understand the fundamental processes occurring on the catalyst surface during FTS.

In addition to optimizing conditions for Co and studying the elemental FTS steps, there is much research into the modification of catalysts with metal oxide promoters, which can alter reaction rates, product distribution, and catalyst stability. A promoter of particular interest is Mn.[9-14] Almost all studies agree that Mn-oxide (MnO_x) promotion increases catalyst activity, decreases methane formation, and enhances the formation of C_{5+} products. How MnO_x promotes the activity is usually associated with the increase in CO adsorption energy on the surface.[13,15-17] To access this claim, we here use a surface science approach by means of APXPS measurements of CO adsorption on a MnO_x modified Co foil in the 10^{-6} – 1 mbar pressure range. The sample temperature was kept at room temperature in order to compensate for the relatively lower pressure and to reach the CO coverage relevant to industrial conditions. We show that the C 1s binding energy of adsorbed CO is lower for Co surfaces partially covered with MnO_x than for pure Co, which is usually a manifestation of stronger CO adsorption (via more π-backdonation) and thus better Coulomb screening. However, we also find that the CO coverage on MnO_x covered Co is less than that on pure Co. This effect is due to hydroxyl groups (either from background water or from background H_2 reacting with CO on the surface to form H_2O) more strongly adsorbing on a MnO_x/Co surface than CO, and covering most of the surface. We found that MnO_x layers on Co promotes the adsorption of both CO and OH, but OH more significantly.

2. Experimental

All the APXPS experiments were performed at the Center for Functional Nanomaterials at Brookhaven National Laboratory. Both sample preparation and XPS measurements were performed in a commercial lab-based ambient pressure photoelectron spectrometer by SPECS Surface Nano Analysis GmbH. The system has a sample preparation chamber and an analysis chamber separated by a gate valve; the base pressure in both chambers is better than 10^{-9} mbar.

Co foils (purity 99.99% on metal basis; temper as rolled, 0.1 mm thick) were cleaned via several cycles of 1 keV Ar^+ sputtering and annealing at 200 °C to remove the implanted Ar. Scanning electron microscopy (SEM) images of course-polished polycrystalline Co foil after preparation are shown in the Figure S1 of the Supporting Information (SI). The surface appears rough. Mn (purity 99.9% on metal basis; powder metallurgy) was deposited on Co foil using e-beam evaporation at low rates. Prior to deposition of Mn on the surface, the evaporator was run for 10 minutes with a closed shutter to remove the native oxide layer from the Mn evaporation rods. We prepared 5 samples with different deposition times: 0 min, 3 min, 10 min, and 35 min at slow rates, 60 min with higher deposition rate. The surface layers of the first and the last samples contained no Mn and no Co, respectively. Other deposition times yielded 93 at.% Co – 7 at.% Mn for 3 min deposition, 79 at.% Co – 21 at.% Mn for 10 min deposition, and 69 at.% Co – 31 at.% Mn for 35 min deposition based on XPS intensity analysis. These atomic percentage values are not the nominal surface coverage of Mn, because the photoelectrons that arise from Co 2p and Mn 2p species are averaged over a few nm depth. However, the overall trend of increasing Mn surface coverage for longer deposition time still holds. In the rest of the paper, we refer to the qualitative and relative coverage of Mn on the surface based on atomic percentage analysis; exact nominal coverage is unknown. Mn appeared dominantly as an oxide because an uncovered metallic Mn surface is highly reactive, even with the low-concentration background gases in ultra-high vacuum (UHV), such as water vapor.

Hydrocarbons or any other contamination/impurities (sulfur, phosphorus, calcium, etc.) that are sometimes encountered in surface science experiments block CO adsorption sites to a great extent. No elements other than Co, Mn, C, and O were present on the surface throughout the experiments. As-prepared samples were not covered with hydrocarbons (measured at 284.4 eV XPS binding energy in the present work – Figure S2), and we did not observe adventitious hydrocarbon accumulation on the model catalyst surfaces throughout the experiments (Figure S3). However, there is a carbide peak throughout the experiments, which originates from the carbon inside the Co film that could not be removed via standard sample cleaning.

To collect XPS data, the sample is placed 600 μm from an aperture (300 μm diameter) that leads to a differential pumping system that permits pressures up to ~ 10 mbar in the analysis chamber. The pumping system also contains a series of electrostatic lenses to focus the photoelectrons into a PHIOBOS 150 NAP hemispherical analyzer. The excitation source is a monochromated Al K_α (E_{hv}=1486.6 eV) anode that is focused to a 300 μm spot. A pass energy of 20 eV was used for the core

level regions. Scofield sensitivity factors were used to account for the photoionization cross sections at different kinetic energies for the relative intensity analysis.[18] We used Mn 2p to Mn 2s intensity ratio for a fully Mn covered surface to estimate the ratio of the analyzer transmission at kinetic energies corresponding to Mn 2p and Co 2p, since Mn 2s and Co 2p have similar binding energies. All the measurements were performed at room temperature.

3. Results and Discussion

To determine the effect of Mn on CO adsorption on the common FTS catalyst Co, different amounts of Mn were deposited on a Co foil. APXPS was used to monitor the CO adsorption sites and relative coverage on the model catalyst surfaces. We start our analysis by determining the chemical state of the surface, as the chemical state affects the CO peak positions and adsorption trends. The XPS spot size is larger than the grain size of the polycrystalline Co foil, therefore the information is averaged over all crystal orientations of the surface.

3.1 Surface Chemical State

The surface after a 3 min Mn deposition is used here as an example to assign peaks in the Co 2p, Mn 2p, Co 3p, and Mn 3p regions and to estimate the changes in the oxidization state of the surface. Spectra acquired on other surfaces with different Mn deposition times are shown in Figures S6-S10. The peak positions are similar in each case.

Figure 1a shows a set of Co $2p_{3/2}$ regions that is used to determine the oxidation state of Co throughout the experiments. Figure 1b is a close-up look to one of the spectra after Shirley background subtraction for better visualization.[19] There are three groups of peaks which are fit with seven components according to Ref.[20]. The Mn 2s core level occurs around 770 eV but has negligible contribution to these spectra. The yellow curve is an Auger line of Co. Red curves are asymmetric and represent metallic Co with the main peak at 778.3 eV and two weak satellites at higher binding energies. Blue curves are symmetric and broader and represent CoO with the main peak at 780.1 eV and two satellites at higher binding energies. Despite CoO and Co_3O_4 having similar positions for the main peak and the first satellite peak (CoO_{sat1}), the second strong satellite feature at around 786.6 eV (CoO_{sat2}) is the signature feature of CoO and confirms this oxide in our spectra.[20]. $Co(OH)_2$ XPS features are similar to those of CoO, as the electronic structure of the d-states in the Co valence band is similar for both species. According to Ref.[20], the CoO main peak and the second satellite peak (the most distinct peaks in our spectra) should appear at 780.0 eV and 786.5 eV, respectively; these features appear at 780.4 eV and 786.0 eV for $Co(OH)_2$. Therefore, we conclude that the red curves represent CoO, and no higher oxidation states of Co or $Co(OH)_2$.

Figure 1c shows the ratio of metallic Co to CoO obtained using spectra in Figure 1a. Similar analysis for other Co 2p spectra are shown in Figure S7. Except at 1 mbar of CO pressure, the Co surface is dominantly metallic (over 90%), regardless of the amount Mn on the surface. In these experiments, photoelectrons that arise from Co 2p and Mn 2p species have an inelastic mean free path (IMFP) of over 1 nm. With signal from this depth, the oxidation state information is averaged over the surface and

several subsurface layers. The oxide intensity of the surface presented here is therefore most likely an underestimation (i.e., it is possible that the entire first Co layer on the surface is CoO at 1 mbar CO).

Initially, it seems peculiar that the Co surface is oxidized more in the presence of 1 mbar CO (Figure 1c) than at lower CO pressures since CO is a reducing molecule. We observed similar behavior in our previous study on metallic Co foil,[8] and attributed it to water impurities. In the present case, we also attribute the oxidation of Co to water impurities that desorb from the chamber walls as CO adsorbs to the walls. Another source of water in the chamber could come from the reaction of CO and H_2, the main component of UHV background gases; the surface is a highly active catalyst for this reaction, producing H_2O at room temperature. Regardless of the water source, we have observed that 10^{-5} mbar of H_2O fully oxidizes Co at room temperature.[8] Additionally, we found that CO reduces CoO above 150 °C in the mbar pressure range.[8] Thus, the current observation of oxidized Co at higher CO pressures matches observations of our previous study. The effect of water impurities is discussed more in Section 3.4.

Figure 2a shows a set of Mn 2p spectra at several CO pressures; the rest of the spectra are shown in Figure S10. As deposited, Mn is a mixture of metallic Mn ($2p_{3/2}$ at 638.8 ± 0.1 eV) and oxidic Mn ($2p_{3/2}$ at 641.3 ± 0.1 eV). More metallic Mn occurs at higher surface coverages (Figure S10d). Metallic Mn atoms are very reactive towards oxidation and readily react with UHV-background gases like H_2O vapor. We can conclude that most topmost Mn atom on the surface is oxidic, whereas Mn atoms beneath the first layer are metallic. Oxidic Mn, as deposited, can be either MnO or Mn_2O_3, as both oxides have the same Mn 2p binding energy. The strong satellite feature at ~647 eV is unique to MnO, suggesting this oxide could be the dominant oxide species in vacuum. In the presence of CO, the metallic peak disappears, and the satellite feature diminishes. Both suggest a transformation of a MnO + Mn mixture to Mn_2O_3. Although this behavior appears counter-intuitive; the likely cause of this oxidation is the water vapor impurities in CO gas and analysis chamber, as previously mentioned in the case of Co oxidation. The oxidation is more severe for Mn than for Co, as this surface is much more reactive. In fact, this behavior is most prominent on the surface fully covered with Mn (Figure S10d), where the metal to oxide intensity decreases from 59% to 52% at 10^{-6} mbar CO, and to roughly 2% at 1 mbar CO.

Figure 2b shows a set of Co 3p and Mn 3p spectra at different CO pressures. Co 3p appears at ~59.0 eV and Mn 3p appears at ~48.1 eV; in both cases the spin-orbit splitting is incompletely resolved.[21] Other spectra in this region are shown in Figure S8. Although the photoelectrons of this region have an IMFP of roughly 2 nm, the direct comparison of Co 3p to Mn 3p intensity can be used to estimate the changes in the surface composition. For instance, a clear increase in the Mn 3p to Co 3p intensity ratio would mean that Mn deposits are conforming flatter to the surface upon CO adsorption. However, we observe only slight changes within the error range which can be due to the changes in background shape due to presence of the CO gas, changes in the intensities of the satellite peaks, CO adsorption attenuating the signal from Co and Mn, etc. Therefore, it is not possible to draw any important conclusions from the Co 3p – Mn 2p region.

3.2 Identification of C and O Species

The CO adsorption can be monitored both in the O 1s and C 1s regions of the XPS spectrum; however, performing the analysis on the C 1s region has two main advantages over analysis based on O 1s region. Firstly, CO adsorbs with C pointing down (more electron transfer from and to molecular orbitals around the C atom), so the peak positions in the C 1s should be affected more than the O 1s peak position. Secondly, in the O 1s region the adsorbed OH peak position and adsorbed CO peak positions are usually similar; hence, their deconvolution is not straightforward.[8]

Figure 3 shows two sets of C 1s data: CO adsorption as a function of CO pressure and as a function of the amount of Mn on the surface. The complete dataset of C 1s spectra are shown in Figure S4. We used slightly assymetric lineshapes for the CO species because of their interaction with the d-electrons close to Fermi level and because of the vibrational losses which should appear as an assymetric tail when the energy resolution is 0.1 eV or worse.[22] The Doniach-Šunjić-like lineshapes of these peaks were constrained with boundaries in the rest of our analysis, whereas the peak positions were not strictly constrained to account for slight shifts in peak positions that are explained later. There are four distinct features in the spectra. The peak above 291 eV is gas phase CO, and its position depends largely on the work function of the surface. The peak at 283.4 ± 0.1 eV is due to carbide contamination inside the Co foil that could not be removed via typical Ar sputtering and annealing cycles. Two types of CO species appear on the surface. The peak at 284.8-285.8 eV is due to CO adsorbed on a metal (CO_m), mostly on metallic Co. Its position depends on the CO pressure, which is at a lower binding energy at 1 mbar compared to the other pressures (Figure 3a). The peak position also depends on the MnO_x surface coverage. The binding energy of this peak is highest on the bare Co and decreases as the MnO_x coverage increases except for the fully Mn covered surface (Figure 3b). The second adsorbed CO species appears at 288.2 eV-290.5 eV, which corresponds CO adsorbed on an oxide (CO_{ox}).[8,23] This peak position again shifts to lower binding energies upon higher CO pressures, but in contrast to the CO_m peak, the CO_{ox} peak increases in binding energy with increasing MnO_x coverage. With these spectra, we conclude that the role of MnO_x is not only electronic changes on Co sites, but it also serves as a CO adsorption site itself. We discuss the CO adsorption trends more in Section 3.3.

3.3 CO Adsorption Trends

CO adsorption trends can be analyzed in terms of the XPS binding energy position in the C 1s region and the normalized XPS intensities. Figure 4a shows the binding energy for CO adsorbed on a metallic site at all the CO pressures measured and for all the prepared surfaces (black '+' signs). As mentioned above, we expect the Mn surfaces to be oxidized, thus CO_m species occur at Co binding sites. At each surface, the lowest binding energy is measured at 1 mbar CO. The red '×' signs are the average of all data obtained for each surface. The binding energy of CO adsorbed on Co decreases from 285.6 eV on average to 285.2 eV on average in the C 1s region once the surface is covered with some MnO_x. This shift is likely due to an electronic effect. In the literature, it has been suggested that at the metal/metal oxide interface, the promotion is via the Mn^{n+} atoms exposed at the edge of the oxides which act as

Lewis acids and enhance the adsorption of CO [13,16,24]. However, the explanation varies. In the original paper where Lewis acidity was suggested as the origin of the promotion effect, adsorbed CO at the oxide/metal interface is bound simultaneously through its C atom to the catalyst metal and its O atom to the Lewis acidic oxide promoter.[24] In another paper, MnO_x acts as an electronic promoter on the Co^0 surface sites, as Mn^{n+} withdraws electron density from the Co^0 sites and produces a relatively greater amount of linearly bonded CO on the Co^0 sites.[13] However, the authors could not detect a discernible blue-shift in the CO stretch frequency, which would have indicated a lower electron density on the Co sites within the classical σ-donation / π-backdonation adsorption mechanism. Irrespective of the exact mechanism, CO adsorbs stronger when a MnO_x/Co interface is present. In our XPS experiments, the C 1s electrons feel somehow a weaker Coulomb interaction upon stronger adsorption, because the carbon nucleus is screened from the C 1s shell through the valence electrons of the metal. This transpires as a lower C 1s binding energy. Thus, like the other authors, we also conclude that CO adsorbs stronger on Co in the presence of some MnO. Core level XPS spectroscopy is an indirect technique for this purpose; Auger-electron yield x-ray absorption spectroscopy at the C K-edge might give more direct information about the 2π*- and 5σ*-derived bands of the adsorbed CO.[25] Similarly, photoelectron spectroscopy at ambient pressures using ultraviolet light sources (UPS) could give more information about the changes in the valence band, especially the newly formed 2π-derived band, [26] although the d-bands will be the most dominant features in these convoluted spectra. At 1 bar CO, the CO_m peak even starts appearing below 285 eV, which has to be related to Mn_2O_3 formation on the surface; and the same mechanism that enhances CO adsorption still holds. On a fully Mn covered surface, the CO_m peak appears at 285.4 eV on average, which might be due to CO adsorbing on the metallic Mn sites. This hypothesis, however, contradicts with our assumption that the exposed Mn surface is always covered with a layer of oxide. The reason for CO adsorbing on metallic Mn sites is currently unclear, but we might speculate these sites to be a small population of edge (low-coordinated) sites which are Mn terminated.

Figure 4b shows the CO adsorption on oxidic sites (can be either MnO_x or CoO). CO adsorption on an oxidic site is below the detection limit for the pure Co surface, despite a CoO to Co^0 ratio of ~1:9 at 1 mbar CO. As the MnO_x amount increases on the surface, CO starts to adsorb on the oxidic sites, but at low Mn coverage (7 at.%) it requires 1 mbar of CO to detect this type of CO. At higher Mn coverage, CO starts adsorbing on oxidic sites at lower pressures: 10^{-2} mbar for 21 at.% Mn, and it readily adsorbs on 31 at.% Mn due to CO in the background from the previous experiments. The binding energy of CO_{ox} also depends on the amount of Mn deposition: 289.2 eV at low Mn coverage with an increase to 290.2 eV at full Mn coverage. One way of interpreting this result is to assume that CO also adsorbs on the CoO sites (at low Mn coverage, there is more CoO than MnO_x on the surface), which appeared at 289.0 eV in Ref.[8]. However, as shown in Figure 3b-i, CO/CoO is below the detection limit in this study. Instead, the increasing binding energy trend of CO/MnO_x (Figure 4b) should be related to the hybridization of MnO_x electronic states with the underlying Co d-states. A simple explanation is MnO_x islands starting to form multilayers on the surface, hence less screening of the carbon nucleus (of CO)

from the C 1s shell through the valence electrons. In more simplified terms, as the MnO_x layer thickness increases, CO starts adsorbing on an oxide with less hybridized character.

Figures 4c (at 10^{-6} mbar CO) and 4d (at 1 mbar CO) show the CO C 1s intensity normalized by dividing it by the sum of Co 2p and Mn 2p (both metallic and oxidic) peak area. In the latter case, background H_2O partially oxidizes the surface, but the surface remains metallic in the former case. Other similar graphs can be found in Figure S5. This normalization is necessary to account for intensity changes during each data collection and signal attenuation due to scattering by gas phase molecules. The y-scales of these graphs are linearly proportional to the actual CO coverage on the surface. Both in Figure 4c and Figure 4d, the CO coverage is low for the moderately MnO_x covered Co surfaces. This contradicts with our and other authors' claim of MnO enhancing CO adsorption on the surface. However, we think these trends in Figure 4c and 4d are not an intrinsic property of the MnO_x/Co surface, but rather due to existence of water impurities, which is discussed in the next section.

3.4 Coadsorption of Water

Our previous analysis suggests the water impurities in the background play an essential role in oxidation of Co and Mn (Section 3.1) and in CO coverage (Section 3.3). For the latter, OH groups must be competing for adsorption sites with CO. To account for the OH on the surface, we analyzed the O 1s spectra. A set of O 1s core level spectra under several CO pressures are shown in Figure 5a for a low Mn coverage sample (Mn deposition for 3 min); the spectra of the other sample preparations are shown in Figure S11. The spectra have three features. The peak at 538 eV is the gas phase CO. The peak at 529.6-529.9 eV is due to either atomic oxygen on the surface or due to lattice oxygen in CoO or MnO_x.[8] The intensity of this peak increases with increasing CO pressure, as more H_2O desorbs from chamber walls and oxidizes the Co and Mn surfaces. The third peak appears at 531.6-532.3 eV and it is due to a convolution of peaks from adsorbed CO or OH species. The binding energy of this peak is lower when there are more OH than CO on the surface.

The relative coverage of each species can be estimated from the C 1s and O 1s spectra. Using the C 1s to O 1s ratio for peaks arising from gas phase CO (which remains consistent throughout the experiments) as a reference, the amount of O 1s intensity corresponding to adsorbed CO can be calculated from the intensity of the adsorbed CO in the C 1s spectrum. Figure 5b shows the results of these estimations for this sample, and the rest are shown in Figure S12. OH groups clearly occupy more adsorption sites than CO at 1 mbar. From Figure S12, the dominance of OH groups over CO is observed only on MnO_x covered surfaces, as the amount of OH groups increases more than the amount of CO as the MnO_x amount increases. This behavior is the reason for the trends seen in Figure 4c and 4d: MnO_x indeed causes a stronger CO adsorption, but it also causes a stronger OH adsorption on the surface. The latter is more significant, hence the higher OH coverage despite the background water pressure being ~6-8 orders of magnitude difference compared to the CO pressure.

Finally, we would like to discuss an alternative explanation. OH could bind more strongly to MnO_x, hence, with more MnO_x on the surface, more OH groups bind, and there are fewer sites available

for CO adsorption. This possibility does not explain the full picture. Figure S12 shows that the amount of OH on the surface does not scale proportionally with the amount of MnO_x on the surface; in fact, in the presence of 1 mbar CO, there are slightly more OH groups on moderately MnO_x covered surfaces than fully MnO_x covered surface. Therefore, the only remaining explanation of the observed trends is that OH adsorbs strongly on MnO_x, but, more importantly, it adsorbs strongly to Co if there is MnO_x present on the surface.

4. Conclusions

In this work, by using APXPS in the 10^{-6} – 1 mbar CO pressure range at room temperature, we found that CO adsorbs on both Co sites and on MnO_x sites on the model MnO_x/Co FTS catalyst surface. However, OH groups formed from background gases in the UHV chamber compete for CO coverage on the surfaces covered with MnO_x. In other words, the same or a similar promotion mechanism is responsible of stronger CO and OH adsorption; but despite water vapor being orders of magnitude less than CO in the gas phase, OH species dominate the XPS spectra. Both Co and Mn are also oxidized by the presence of water vapor.

Water is important in FTS, as it is a product of the reaction. Other than the importance of our results for the FTS and catalysis community, it also highlights an 'elephant in the room' in the ambient pressure surface science studies: There are more impurities in the background (especially H_2O) than in traditional surface science studies in UHV. Their contribution to XPS spectra (or to other spectroscopy and microscopy techniques) cannot be ignored and must be taken into account in each case. A similar conclusion was drawn in a recent paper, which shows oxygenated hydrocarbons to accumulate on oxidized copper surfaces in the presence of water vapor.[27]

Supporting Information

The Supporting Information is available free of charge on the ACS Publications website.

All the APXPS spectra in the C 1s, O 1s and Co 2p regions and their analysis. Scanning electron microscopy images of the sputtered Co surface. Comparison of the C 1s spectra of hydrocarbon contaminated surface and a cleaner surface.

Acknowledgements

This work was supported by Israel Science Foundation's (ISF) grant no. 919/18. This research used resources of the Center for Functional Nanomaterials, which is a U.S. DOE Office of Science Facility, at Brookhaven National Laboratory under Contract No. DE-SC0012704. BE acknowledges the support from the Zuckerman STEM Leadership Faculty Fellowship, Ruth and Herman Albert Scholarship Program for New Scientists, and the Abramson Family Center for Young Scientists.

Figures:

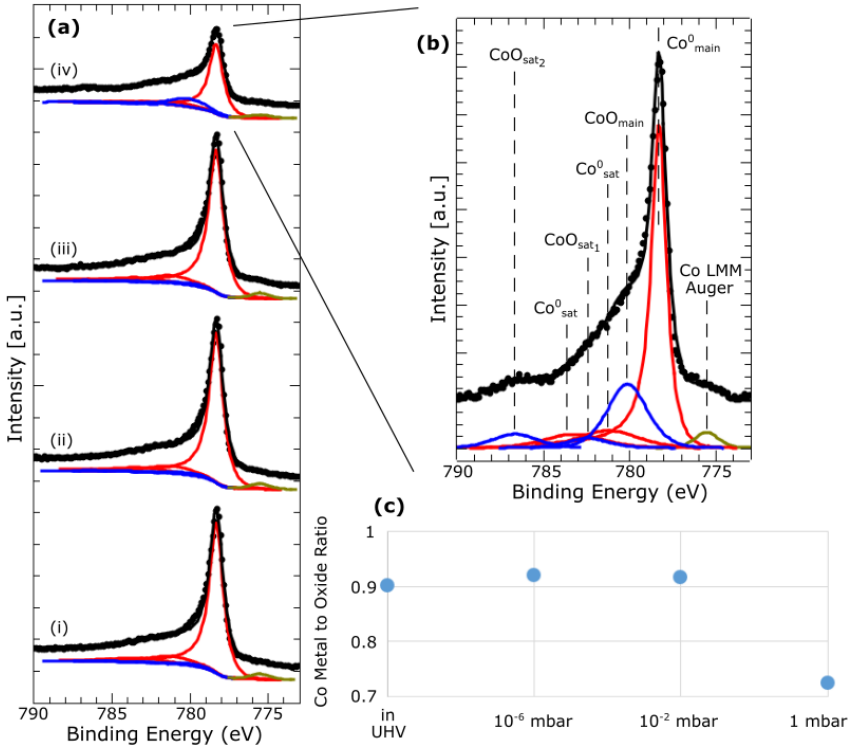

Figure 1 (a) Example of a set of Co $2p_{3/2}$ spectra for 3 min Mn deposition on Co (93 at.% Co, 7 at.% Mn); spectra for other deposition times are shown in Figure S6. (i) in UHV, (ii) in the presence of 10^{-6} mbar CO, (iii) 10^{-2} mbar CO, and (iv) 1 mbar CO. The chemical state analysis discussed in Section 3.1 is done using the Co $2p_{3/2}$ spectra, which is fit with 7 components. (b) Enlarged Co $2p_{3/2}$ region details the fit: The yellow curve is an Auger line of Co. Red curves are asymmetric and represent metallic Co with the main peak at 778.3 eV and two weak satellites at higher binding energies. Blue curves are symmetric and broader, and represent CoO with the main peak at 780.1 eV and two satellites at higher binding energies. Fitting for all the XPS peaks were done in accordance with Ref.[20]. (c) The Co to oxidic Co ratio based on the spectra are plotted versus pressure. Similar analysis at other pressures are shown in Figure S7.

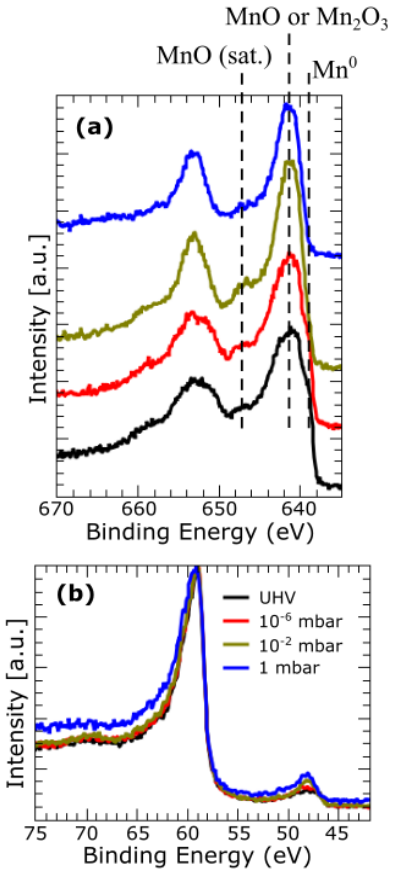

Figure 2 Example of a set of (a) Mn 2p spectra, and of (b) Co 3p – Mn 3p spectra, for 10 min Mn deposition on Co; spectra for other deposition times are shown in Figure S10 and S8. The color code in (b) also applies to (a). In (a), it can be observed that Mn is a mixture of metallic Mn (638.8 ± 0.1 eV) and oxidic Mn (MnO or Mn_2O_3 at 641.3 ± 0.1 eV). The satellite feature (~647 eV) is a feature of MnO, so the weaker that feature more oxidized the surface is from MnO to Mn_2O_3. In (b), Mn 3p is located at ~48.1 eV and Co 3p is at ~58.0 eV.

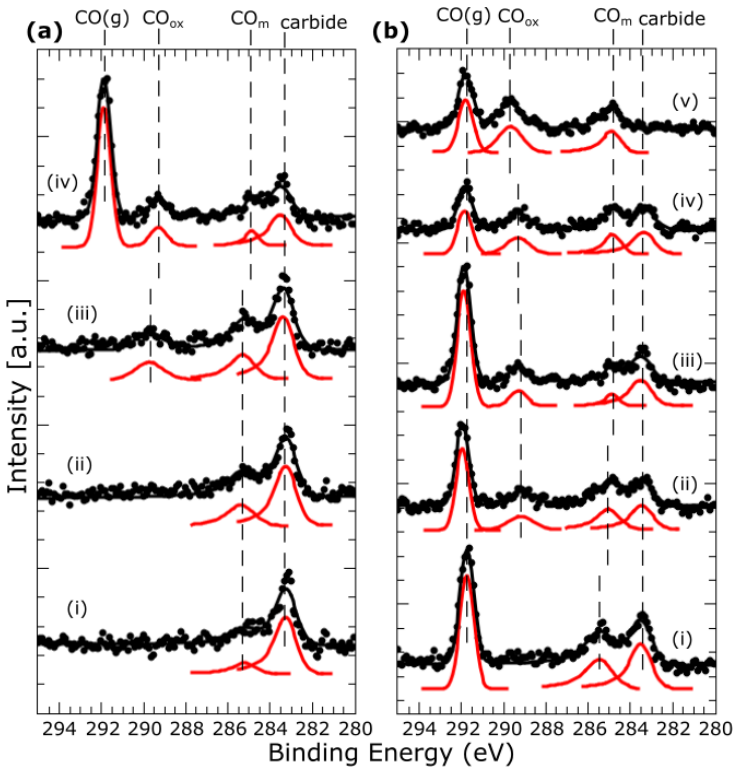

Figure 3 Two sets of C 1s region of the XPS spectra: (a) The surface obtained after 10 min of Mn deposition (79 at.% Co, 21 at.% Mn), as a function of pressure (i) background adsorption, (ii) in the presence of 10^{-6} mbar CO, (iii) 10^{-2} mbar CO, and (iv) 1 mbar CO. (b) As a function of the Mn surface population in the presence of 1 mbar CO: (i) pure Co, (ii) after 3 min Mn deposition (93% at. Co - 7% at. Mn), (iii) after 10 min Mn deposition (79% at. Co - 21% at. Mn), (iv) after 35 min Mn deposition (69% at. Co - 31% at. Mn), and (v) fully covered Mn surface. Rest of the C 1s spectra are shown in Figure S4. The peak above 291 eV is gas phase CO, and its position depends largely on the work function of the surface. The peak at 283.4 ± 0.1 eV is due to carbide contamination inside the Co foil. CO species appear at two different position: The peak at 284.8-285.8 eV is due to CO on a metal (CO_m), mostly on metallic Co. Its position depends on the CO pressure and the MnO_x coverage on the surface. The second CO peak appears at 288.2 eV-290.5 eV, which is CO on an oxide (CO_{ox}); mostly on MnO_x.

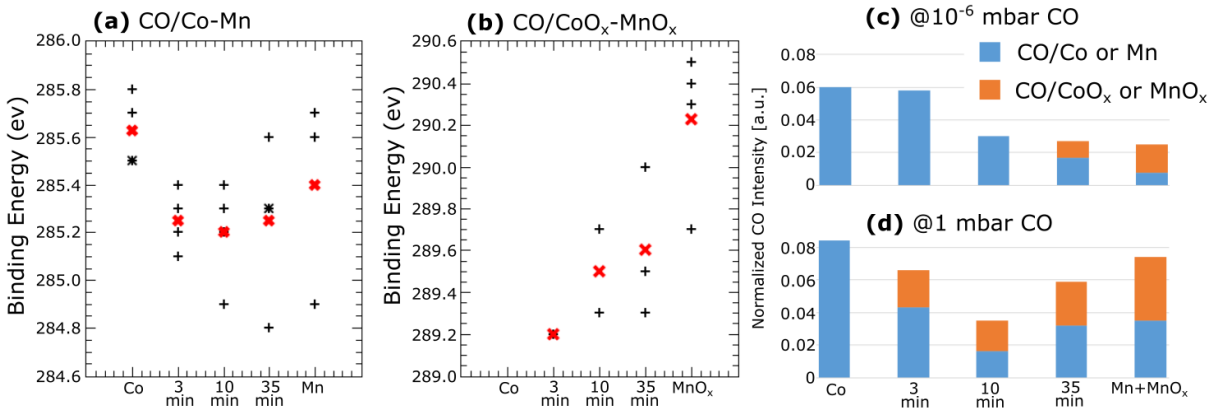

Figure 4 Trends of the XPS binding energies in the C 1s range: (a) CO on metallic sites; mostly on Co, (b) CO on oxide sites; mostly on MnO_x. Each data point is a '+' sign, and the red '×' signs are the average of all data obtained for each surface under several CO pressures. In (a), the decrease in the C 1s binding energy is due to the presence of MnO_x (except for the fully Mn-covered surface). In (b), the increase in the C 1s binding energy is related to the hybridization of the Co and MnO_x electronic states. (c) and (d) show the CO coverage on metallic and oxidic surfaces at 10^{-6} mbar CO and at 1 mbar CO. Similar analysis for other pressures are shown in Figure S5. Whilst in the latter case, background H_2O partially oxidizes the surface, the surface remains metallic in the former case. In both cases, however, the CO coverage is less for moderately MnO_x covered surfaces (e.g., 10 min deposition; 21 at.% Mn) than that of pure Co.

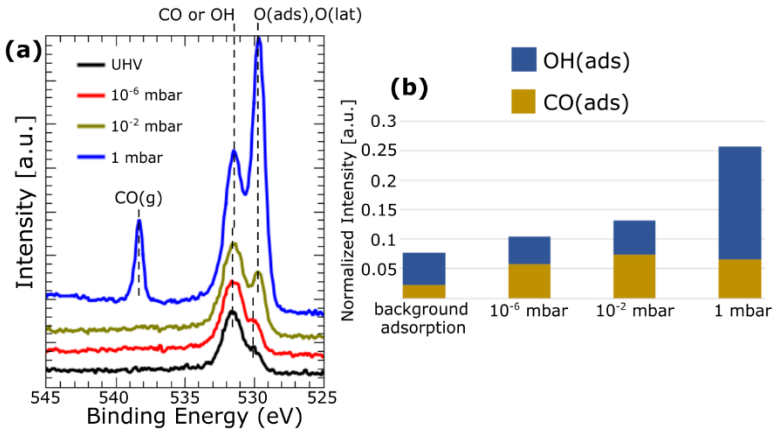

Figure 5 (a) Example of an O 1s region of the XPS spectra acquired for the Co surface covered with MnO_x deposited for 3 minutes at different CO pressures. The peak over 538 eV arises due to the gas phase CO. The peak on 529.6-529.9 eV is due to adsorbed oxygen or lattice oxygen. The peak at 531.6-532.3 eV is due to a convolution of peaks due to adsorbed CO or OH species. The measured XPS binding energy is slightly lower when there is more OH^- on the surface. (b) is the constructed CO and OH normalized intensities on the surface by using O 1s to C 1s ratio of gas phase CO to estimate the OH amount. Similar spectra and analysis for other surfaces are shown in Figure S11 and S12. Except for pure Co, OH groups due to background water is very significant and at higher pressures more dominant than CO on the surface.

References:

[1] Fischer, F.; Tropsch, H. Über die Herstellung Synthetischer Ölgemische (Synthol) durch Aufbau aus Kohlenoxyd und Wasserstoff. *Brennstoff-Chemie* **1923**, *4*, 276−285.

[2] Bell, A. T. Catalytic Synthesis of Hydrocarbons over Group VIII Metals. A Discussion of the Reaction Mechanism. *Catal. Rev. – Sci. Eng.* **1981**, *2*, 203−232.

[3] Iglesia, E.; Reyes, S. C.; Madon, R. J.; Soled, S. L. Selectivity Control and Catalyst Design in the Fischer-Tropsch Synthesis: Sites, Pellets, and Reactors. *Adv. Catal.* **1993**, *39*, 221−302.

[4] Khodakov, A. Y.; Chu, W.; Fongarland, P. Advances in the Development of Novel Cobalt Fischer−Tropsch Catalysts for Synthesis of Long-Chain Hydrocarbons and Clean Fuels. *Chem. Rev.* **2007**, *107*, 1692−1744.

[5] Iglesia, E. Design, Synthesis, and Use of Cobalt-based Fischer-Tropsch Synthesis Catalysts. *Appl. Catal. A*, **1997**, *161*, 59−78.

[6] Zhang, Y.; Liu, Y.; Yang, G.H.; Sun, S. L.; Tsubaki, N. Effects of Impregnation Solvent on Co/Sio_2 Catalyst For Fischer-Tropsch Synthesis: A Highly Active and Stable Catalyst with Bimodal Sized Cobalt Particles. *Appl. Catal. A* **2007**, *321*, 79−85.

[7] Bian, G. Z.; Mochizuki, T.; Fujishita, N.; Nomoto, H.; Yamada, M. Activation and Catalytic Behavior of Several Co/SiO_2 Catalysts for Fischer−Tropsch Synthesis. *Energy Fuels* **2003**, *17*, 799-803.

[8] Wu, C. H.; Eren, B.; Bluhm, H.; Salmeron, M. Ambient-Pressure X-ray Photoelectron Spectroscopy Study of Cobalt Foil Model Catalyst under CO, H_2, and Their Mixtures. *ACS Catalysis* **2017**, *7*, 1150−1157.

[9] Feltes, T. E.; Espinosa-Alonso, L.; de Smit, E.; D'Souza, L.; Meyer, R. J.; Weckhuysen, B. M. Regalbuto, J. Selective Adsorption of Manganese onto Cobalt for Optimized $Mn/Co/TiO_2$ Fischer–Tropsch Catalysts. *J. Catal.* **2010**, *270*, 95−102.

[10] den Breejen, J. P.; Frey, A.M.; Yang, J.; Holmen, A.; van Schooneveld, M. M.; de Groot, F. M. F.; Stephan, O.; Bitter, J. H.; de Jong, K. P. A. Highly Active and Selective Manganese Oxide Promoted Cobalt-on-Silica Fischer–Tropsch Catalyst. *Top. Catal.* **2011**, *54*, 768−777.

[11] Morales, F.; de Groot, F. M. F ; Glatzel, P.; Kleimenov, E.; Bluhm, H.; Hävecker, M.; Knop-Gericke, A.; Weckhuysen, B. M. In Situ X-ray Absorption of $Co/Mn/TiO_2$ Catalysts for Fischer-Tropsch Synthesis. *J. Phys. Chem. B* **2004**, *108*, 16201–16207.

[12] Voss, J. M.; Xiang, Y.; Collinge, G.; Perea, D. E.; Kovarik, L.; McEwen, J.-S.; Kruse, N. Characterization of CoCu- and CoMn-Based Catalysts for the Fischer-Tropsch Reaction toward Chain-Lengthened Oxygenates. *Topics in Catal.* **2018**, *61*, 1016–1023.

[13] Morales F.; Smit, E.; de Groot, F. M. F.; Visser, T.; Weckhuysen, B. M. Effects of Manganese Oxide Promoter on the CO and H_2 Adsorption Properties of Titania-supported Cobalt Fischer–Tropsch Catalysts. *J. Catal.* **2007**, *246*, 91–99.

[14] Zhou, W.-G.; Liu, J.-Y.; Wu, X.; Chen, J.-F.; Zhang, Y. An Effective Co/MnOx Catalyst for Forming Light Olefins via Fischer–Tropsch Synthesis. *Catal Comm.* **2015**, *60*, 76–81.
[15] Pedersen, E. Ø.; Svenum, I.-H.; Blekkan, E. A. Mn Promoted Co Catalysts for Fischer-Tropsch Production of Light Olefins – An Experimental and Theoretical Study. *J. Catal.* **2018**, *361*, 23–32.
[16] Dinse, A.; Aigner, M.; Ulbrich, M.; Johnson, G. R.; Bell, A. T. Effects of Mn Promotion on the Activity and Selectivity of Co/SiO_2 for Fischer–Tropsch Synthesis. *J. Catal.* **2012**, *288*, 104–114.
[17] Johnson, G. R.; Werner, S.; Bell, A. T. An Investigation into the Effects of Mn Promotion on the Activity and Selectivity of Co/SiO_2 for Fischer-Tropsch Synthesis: Evidence for Enhanced CO Adsorption and Dissociation. *ACS Catal*. **2015**, *5*, 5888–5903.
[18] Scofield, J. H. Hartree-Slater Subshell Photoionization Cross-sections at 1254 and 1487 eV. *J. Electron Spectrosc.* **1976**, *8*, 129−137.
[19] Shirley, D. A. High-Resolution X-Ray Photoemission Spectrum of the Valence Bands of Gold. *Phys. Rev. B* **1972**, *5*, 4709.
[20] Biesinger, M. C.; Payne, B. P.; Grosvenor, A. P.; Lau, L. W. M.; Gerson, A. R.; Smart, R. S. C. Resolving Surface Chemical States in XPS Analysis of First Row Transition Metals, Oxides and Hydroxides: Cr, Mn, Fe, Co and Ni. *Appl. Surf. Sci.* **2011**, *257*, 2717−2730.
[21] Klebanoff, L. E.; Van Campen, D. G.; Pouliot, R. J. Spin-resolved and High-energy-resolution XPS Studies of Cobalt Metal and a Cobalt Magnetic Glass. *Phys. Rev. B* **1994**, *49*, 2047−2057.
[22] Föhlisch, A.; Wassdahl, N.; Hasselström, J.; Karis, O.; Menzel, D.; Mårtensson, N.; Nilsson, A. Beyond the Chemical Shift: Vibrationally Resolved Core-Level Photoelectron Spectra of Adsorbed CO. *Phys. Rev. Lett.* **1998**, *81*, 1730.
[23] Eren, B.; Heine, Ch.; Bluhm, H.; Somorjai, G. A.; Salmeron, M. Catalyst Chemical State during CO Oxidation Reaction on Cu(111) Studied with Ambient-Pressure X-ray Photoelectron Spectroscopy and Near Edge X-ray Adsorption Fine Structure Spectroscopy. *J. Am. Chem. Soc.* **2015**, *137*, 11186−11190.
24 Boffa, A.B.; Lin, C.;, Bell, A.T.; Somorjai, G. A. Lewis Acidity as an Explanation for Oxide Promotion of Metals: Implications of Its Importance And Limits for Catalytic Reactions. *Catal. Lett.* **1994**, *27*, 243−249.
[25] Stöhr, J. *NEXAFS Spectroscopy*; Springer-Verlag: Berlin, 2003.
[26] Hüfner, S. *Photoelectron Spectroscopy – Principles and Applications*; Springer-Verlag: Berlin, 2003.
[27] Trotochaud, L.; Head, A. R.; Pletincx, S.; Karslıoğlu, O.; Yu, Y.; Waldner, A.; Kyhl, L.; Hauffman, T.; Terryn, H.; Eichhorn, B.; et al. Water Adsorption and Dissociation on Polycrystalline Copper Oxides: Effects of Environmental Contamination and Experimental Protocol. *J. Phys. Chem. B* **2018**, *122*, 1000−1008.

TOC Graphic: